nature biomedical engineering

SUPPLEMENTARY INFORMATION

https://doi.org/10.1038/s41551-020-0534-9

In the format provided by the authors and unedited.

A mountable toilet system for personalized health monitoring via the analysis of excreta

Seung-min Park[1,2,17], Daeyoun D. Won[1,3,4,17], Brian J. Lee[1,2,17], Diego Escobedo[1], Andre Esteva[5], Amin Aalipour[1,2], T. Jessie Ge[6], Jung Ha Kim[3], Susie Suh[7], Elliot H. Choi[7], Alexander X. Lozano[8,9], Chengyang Yao[10], Sunil Bodapati[11], Friso B. Achterberg[1,2,12], Jeesu Kim[1,2,13], Hwan Park[14], Youngjae Choi[14], Woo Jin Kim[14], Jung Ho Yu[1,2], Alexander M. Bhatt[1], Jong Kyun Lee[3,4], Ryan Spitler[1,15], Shan X. Wang[8,10,16] and Sanjiv S. Gambhir[1,2,8,11,15,16] ✉

[1]Department of Radiology, Stanford University School of Medicine, Stanford, CA, USA. [2]Molecular Imaging Program at Stanford, Stanford University School of Medicine, Stanford, CA, USA. [3]Department of Surgery, Seoul Song Do Hospital, Seoul, Republic of Korea. [4]Cancer Immunology Laboratory, Seoul, Seoul Song Do Hospital, Republic of Korea. [5]Salesforce Research, Palo Alto, CA, USA. [6]Department of Urology, Stanford University School of Medicine, Stanford, CA, USA. [7]Department of Pharmacology, Case Western Reserve University School of Medicine, Cleveland, OH, USA. [8]Department of Materials Science and Engineering, Stanford University, Stanford, CA, USA. [9]Faculty of Medicine, University of Toronto, Toronto, Ontario, Canada. [10]Department of Electrical Engineering, Stanford University, Stanford, CA, USA. [11]Department of Bioengineering, Stanford University, Stanford, CA, USA. [12]Department of Surgery, Leiden University Medical Center, Leiden, the Netherlands. [13]Department of Creative IT Engineering, Pohang University of Science and Technology (POSTECH), Pohang, Republic of Korea. [14]College of Medicine, The Catholic University of Korea, Seoul, Republic of Korea. [15]Precision Health and Integrated Diagnostic Center (PHIND), Stanford University School of Medicine, Palo Alto, CA, USA. [16]Canary Center at Stanford for Cancer Early Detection, Stanford University School of Medicine, Palo Alto, CA, USA. [17]These authors contributed equally: Seung-min Park, Daeyoun D. Won, Brian J. Lee.
✉e-mail: sgambhir@stanford.edu

TABLE OF CONTENTS

Bristol Stool Form Scale

The Bristol Stool Form Scale (BSFS), or the Bristol Stool Chart (BSC), is a diagnostic tool used in the identification and classification of human faeces. This particular scale was developed at the Bristol Royal Infirmary in 1997[1], and today, it is the most popular and effective evaluation technique for clinically assessing various bowel conditions. The chart is broken up into seven categories, each of which designates a distinct stool type. For example, "Type 1" is associated with severe constipation while "Type 7" is associated with severe diarrhoea. Over the past 20 years, the BSFS has become the standard-of-care clinical tool around the world among physicians interested in gathering health data from human excreta. The class descriptions are as follows:

Supplementary Table 1. The Bristol Stool Form Scale.

	Description	
Type 1	“Separate hard lumps, like nuts (hard to pass)”	
Type 2	“Sausage-shaped but lumpy”	
Type 3	“Like a sausage but with cracks on the surface”	
Type 4	“Like a sausage or snake, smooth and soft”	
Type 5	“Soft blobs with clear cut edges (passed easily)”	
Type 6	“Fluffy pieces with ragged edges, a mushy stool”	
Type 7	“Watery, no solid pieces, entirely liquid”	

Clinical Applications of BSFS

Functional bowel disorders are recognized as a disease entity that plays a significant clinical and social impact, often affecting patient's quality of life[2]. Irritable bowel syndrome (IBS), the most common functional gastrointestinal (GI) disorder with worldwide prevalence rates of 10 to 15%[3], is one of the best examples showing that toilet system can have profound practical application. Functional disorders such as IBS are conditions in which there is a lack of structural or biochemical abnormalities on routine tests, implying no specific causality. BSFS has been used to describe the stool form and consistency in functional bowel disorders such as IBS, chronic diarrhoea, and chronic constipation. BSFS is included in the Rome diagnostic criteria for IBS and as an objective tool in clinical trials[4]. IBS patients are classified based on the frequency of loose/watery or hard/lumpy stools. Stool consistency reporting is important because IBS drugs are intended to treat either diarrhoea or constipation. BSFS should be used to direct treatment based on the predominant gastrointestinal symptoms[4].

Episodic nature of symptoms in IBS has been reported, and assessment may be difficult because of the fluctuation of periodic symptoms[5]. A notable study showed that 78% of IBS patients of all subtypes fluctuate between the extremes of loose/watery stools and hard/lumpy stools[6]. The study also reported that daily symptom monitoring is more sensitive and reliable than merely a questionnaire. Questionnaires overestimated the frequency of abnormal stool consistency and gastrointestinal symptoms as compared to stool diaries including BSFS.

The image analysis of BSFS in the toilet will add a more accurate assessment of daily stool forms and provide a better means of continuous longitudinal monitoring of bowel movements. It has been shown that there are major disparities between patients' stool descriptions and basic, objective features of constipation/diarrhea[7].

Moreover, there were variances between parent recall and child stool diaries[8], further showing the inherent inaccuracies that emerge from questionnaires. Our system will eliminate human recollection bias, provide automated stool form data collection and endeavour to provide a more precise assessment of bowel movements and serve as a treatment-monitoring tool.

Previous studies noted the rater agreement and reliability of the BSFS (Type 1 - 7) among 34 gastroenterologists from three different institutions. However, the agreement decreased when the stool form was categorized into 3 types (constipation, normal, or diarrhoea) by the Rome criteria. It was hard to distinguish type 2 from type 3 (boundary between normal stool and constipation), and type 5 from type 6 stools (boundary between normal stool and diarrhoea)[9,10]. The image analysis of BSFS in the toilet may provide better pattern recognition around the clinical decision points differentiating BSFS Types 2, 3, 5, and 6.

BSFS also plays a significant role in oncologic outcome assessment. The scale has the ability to assess the functional aspect of patients after surgery, chemotherapy, and radiation therapy. Stool form and frequency have been known to change after gastrointestinal tract resections[11-14]. Furthermore, chemotherapy-induced diarrhoea or constipation can be caused by numerous agents[15,16] and radiation therapy around the pelvic area can cause visible symptoms and lead to significant bowel damage[17]. A gap between physician and patient reported outcome was noted. Similarly, opioid-induced constipation is also a frequent clinical problem faced by clinicians[18-21]. Real time assessment of stool form and frequency, as well as bowel related symptoms, will help provide useful information regarding chemotherapy, opioid drugs, and radiation dose modification.

Minimally invasive surgery has been gaining a larger role in oncologic surgery. Laparoscopic and robotic surgery provide non-inferior oncologic outcomes and better

short-term outcomes. Minimally invasive surgery has better cosmesis, less postoperative pain, less ileus (paralysis of normal intestinal peristalsis), and shorter hospital stay. However, many randomized control trials do not mention the functional advantages of minimally invasive surgery related to urination and defecation. Unfortunately most of these related symptoms will occur outside of the hospital, making it difficult to assess the general view of the patient's activity. Only few trials have provided a cross sectional and fragmented view of patients' symptoms at specific points in time. Questionnaires are provided in time intervals, and the longitudinal monitoring strategy may provide more insight in the long-term functional outcome of minimally invasive surgery.

In summary, the Rome IV criteria[22] integrate the BSFS into guidelines used by clinicians around the world. The Rome IV criteria for IBS are based on the recollection of symptoms in the past 3 months prior to diagnosis, and require symptom onset at least 6 months prior to diagnosis. Thus, additional information regarding the frequency and quality of bowel movements would greatly aid the diagnosis and characterization of a patient's IBS. For example, IBS with constipation presents with hard or lumpy stools in ≥25% of bowel movements, and loose or watery stools <25% of bowel movements. However, bias may be present in a patient's recollection of their bowel movements, and diligently and objectively classifying stool after each and all bowel movements is unduly burdensome and unrealistic, especially for elderly and infirm patients. In addition, the BSFS is clinically used to evaluate the response to anti-diarrheal medications such as loperamide or senna[1] and other medications and therapies (e.g., cholestyramine)[23]. In addition, the BSFS may help guide the management of diarrhoea during chemotherapy. Chemotherapy-induced gastrointestinal toxicity is relatively common and early detection of toxicity is one of

the key factors in cancer patient management in minimizing morbidity by adjusting dosing regimen. Our toilet system has the ability to perform image analysis of stool forms and endeavours to provide a more precise assessment of bowel movements and serve as a treatment-monitoring tool.

Supplementary Table 2. Current and potential disease/state screening that may benefit from the toilet system. The upper part of the table indicates capable disease/state screening with the current version of the toilet. The lower part of the table requires more advanced technology and higher-level system integration. NAAT: Nucleic Acid Amplification Test, BSFS: Bristol Stool Form Scale, AMP: Amphetamine, BAR: Barbiturate, BUP: Buprenorphine, BZO: Benzodiazepines, COC: Cocaine, mAMP: Methamphetamine, MDMA: Methylenedioxymethamphetamine, MTD: Methadone, OPI: Opiate, OXY: Oxycodon, PCP: Phencyclidine, PPX: Propoxyphene, TCA: Tricyclic antidepressants, THC: Tetrahydrocannabinol.

Disease/Symptom	Biomarker/Measurement	Current test		Disease/Symptom	Biomarker/Measurement	Current test
Urination				**Defecation**		
Nocturia (congestive heart failure, sleep apnea)	Frequency, time of day	Urine diary	Current Model	Irritable bowel syndrome (IBS)	Fluctuation in stool frequency, consistency	Stool diary, BSFS
Oligo-/polyuria	Volume	Urine diary		Constipation	Seating time, BSFS, initial stool drop time	Stool diary, BSFS
Benign prostatic hypertrophy	Flow rate vs. duration of urination	Uroflowmetry		Fecal incontinence	Presence of stool in the perianal area, fecal incontinence score	Stool diary, BSFS
Urinary retention (medications, surgery)	Decreased or absent urination	Uroflowmetry		Low anterior resection syndrome	Frequency, initial stool drop time, total toilet sitting time, straining, fecal incontinence score	Stool diary, BSFS
Skin morphology				**Skin morphology**		
Morphological changes to the external genitalia	Non-infectious skin diseases (e.g. Lichen planus/sclerosis, M. Paget), infectious skin disease (e.g. genital warts, balanitis)	Image analysis		Morphological changes to the perineal area	(Traumatic) skin lesion, swelling	Image analysis
Urinalysis				**Stool analysis**		
				<u>Disease monitoring</u>		
Dehydration	Urine volume, color, specific gravity	Strip, uroflowmetry		Chemotoxicity (GI)	Constipation, diarrhea, stool frequency, BSFS	Clinical correlation with chemotherapy
Diabetes	Frequency, glucosuria, proteinuria	Urine diary, strip*		Pseudomembranous colitis (antibiotic related)	BSFS, diarrhea, stool frequency	Colonoscopy, biopsy
Urinary Tract Infection	Frequency, WBC, Nitrites	Strip*		Radiation induced proctitis	BSFS, diarrhea, stool frequency, bleeding	Clinical correlation with radiation therapy
Pregnancy	β-hCG	Strip*		Inflammatory bowel disease (Crohn, ulcerative colitis)	Calpronectin, anal bleeding, diarrhea, perianal skin lesion, symptom severity quantification	Colonoscopy, blood test, biopsy
Ovulation	Progesterone, follicle stimulating hormone (FSH), luteinizing hormone (LH), estrogen	Strip*		Celiac Disease	BSFS (Diarrhea)	Small bowel biopsy
Intrinsic renal disease (e.g. glomerulonephritis, nephrotic syndrome) Ψ	Proteinuria, hematuria, cellular casts	Strip*		Malabsorption	72-hour stool collection, BSFS, color	Lactose hydrogen breath test, fecal fat analysis, fecal bile acid test
Kidney Stones Ψ	Hematuria, pH, mineral levels (calcium, oxalate, citrate, uric acid, sodium, potassium), total volume	Strip*				
				<u>Early detection</u>		
Alcohol	Ethyl glucuronide (EtG), >500 ng/mL	Strip*		Extrahepatic bile duct obstruction	Pale stool color	Fecal bile analysis
Liver dysfunction/ Biliary obstruction Ψ	Bilirubin	Strip*		Steatorrhea	Vitamin A, D, E, K deficiency Fatty stool	Blood test, fecal fat analysis
Cushing Syndrome, Addison's disease Ψ	Cortisol	Lab test		Salmonella, E.coli, Lysteria, C. diff, etc.	BSFS (diarrhea), bacteria/toxins	Stool culture
Illicit Drugs	AMP/BAR/BUP/BZO/COC/mAMP/MDMA/MTD/OPI/OXY/PCP//TCA/THC	Strip*				
Renal Cancer	Hematuria, urine cytology	Strip, Cytology	Future Model	Colon cancer	gFOBT, mucoid stool, thin stool, stool DNA	Colonoscopy, CEA, biopsy
Bladder Cancer	Hematuria, urine cytology, tumor-related proteins or nucleic acids	Strip, Cytology				
Multiple Myeloma Ψ	Proteinuria (Bence Jones protein)	Strip, Lab test				
Sexually transmitted diseases	Chlamydia, Gonorrhea	NAATs				
Prostate Cancer Ψ	Prostate cancer gene 3 & PSA RNA	NAATs				
Urothelial cancer Ψ	Urine cytology	Cytology				

Sensor & Image analysis
Biochemical analysis
Cell (product) analysis
* Commercially available

Ψ The Smart Toilet system might aid in monitoring or creating first awareness

Supplementary Schematics. a. Flowchart view of the toilet system. This system is designed to minimally interfere with human intervention. **b**. Flowchart view of the cloud system.

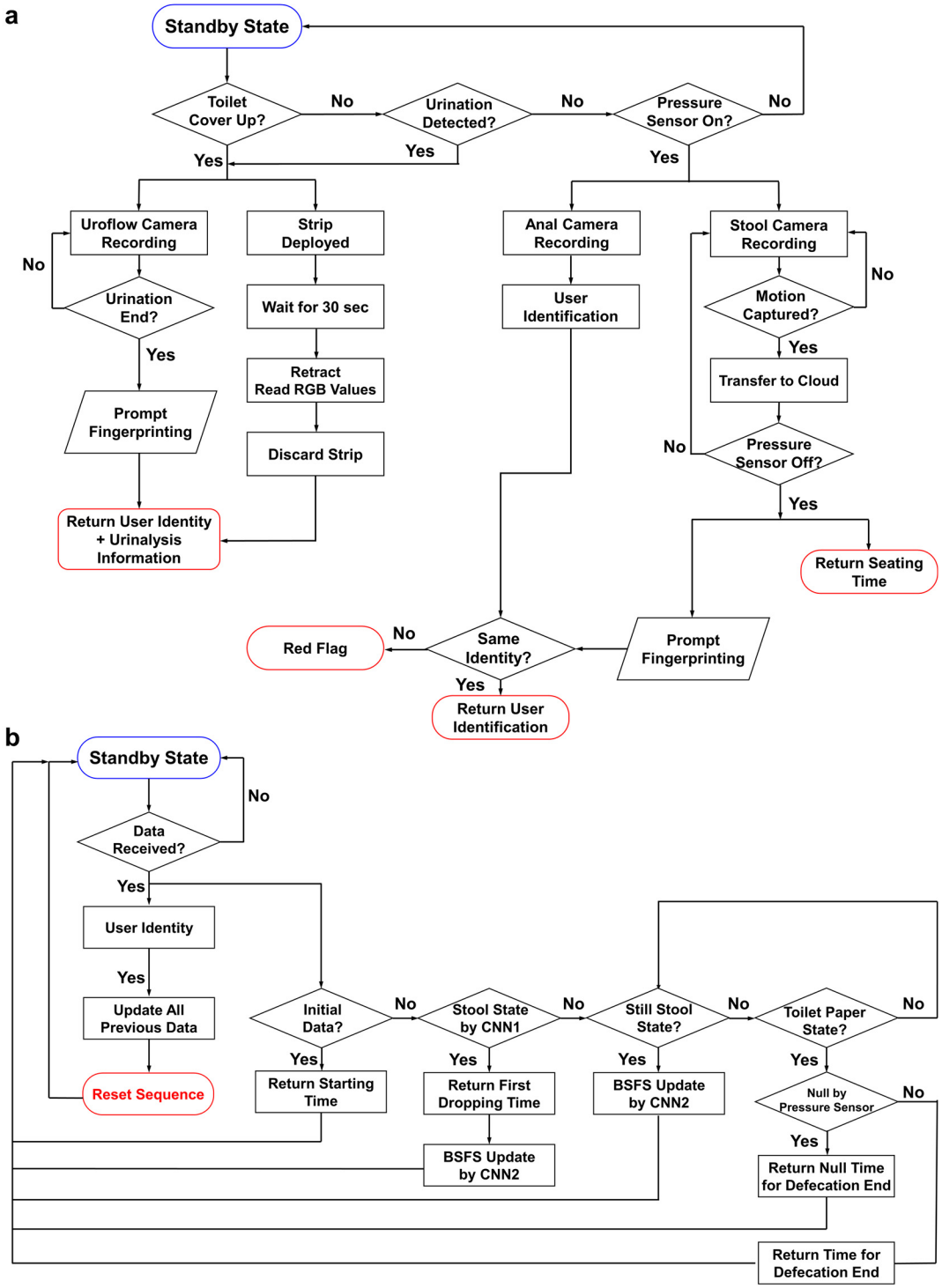

Continuous Monitoring of Human Urination

We tested whether more frequent urinalysis would benefit human health monitoring. We performed continuous monitoring of urination from two research participants with a commercially available 10-parameter urinalysis test strip (Accustrip URS-10 Urine Reagent Strips, Jant Pharmacal Corp., Encino, CA). Two research participants were instructed to use test strips whenever they needed to void. Instead of the dipping method of urinalysis strips, the participants were instructed to urinate directly onto the test strips. There were insignificant differences between the dipping method and direct urination method in our pilot experiments. 133 and 42 measurements (research participant #1 [male, 39-year old] and #2 [female, 39-year old], respectively), were made over the course of one month. One research participant (research participant #2) experienced a urinary tract infection (UTI) with subsequent antibiotic treatment (nitrofurantoin), as reflected in **Supplementary Figure 1**. A subset of urinalysis components (leukocytes and erythrocyte activities) responded to the antibiotic treatment, while the healthy untreated participant showed no change in those components. In addition, another subset of urinalysis components (specific gravity and pH) appears to be very participant-specific.

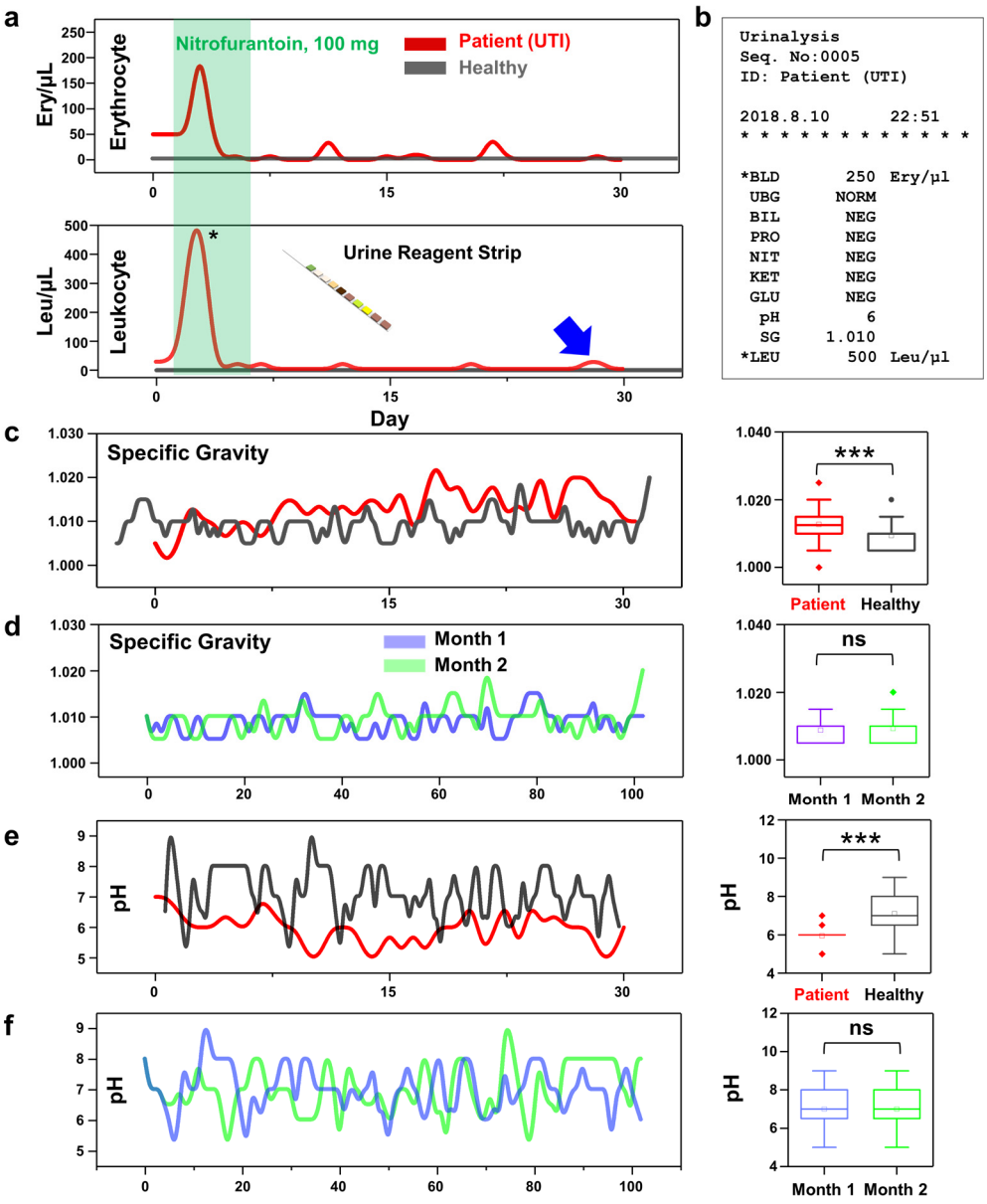

Supplementary Figure 1. Continous monitoring – Urinalysis. Continuous monitoring of participants' urination with a commercially available 10-biomarker dipstick. **a**. Two participants were participating this experiment. 133 and 42 measurements were made over the course of one month. **b**. A typical read-out of urinalysis. These measurements are analyzed with a strip reader. This printed slip is from a time point denoted by the asterisk in **a**. **c**. Specific gravity comparison bewteen the two participants. Their difference was statistically significant (two sample *t* test, *p*-value = 5.63×10^{-6}). **d**. Specific gravity comparison by month between the same participant (#1). There was a statistically insignificant difference (two sample *t* test, *p*-value = 0.02 with a threshold, 0.01). **e**. pH comparision bewteen the two participants. Their difference was statistically significant (two sample *t* test, *p*-value = 9.54×10^{-13}). **f**. pH comparison by month between the same participant (#1). There was a statistically insignificant difference (two sample *t* test, *p*-value = 0.24).

Urinalysis Module

The urinalysis module consists of a retractable urinalysis subunit (**Supplementary Figure 2**) and a real-time colorimetric detector subunit (**Supplementary Figure 3**). The two subunits shown below will ultimately be integrated into the toilet system.

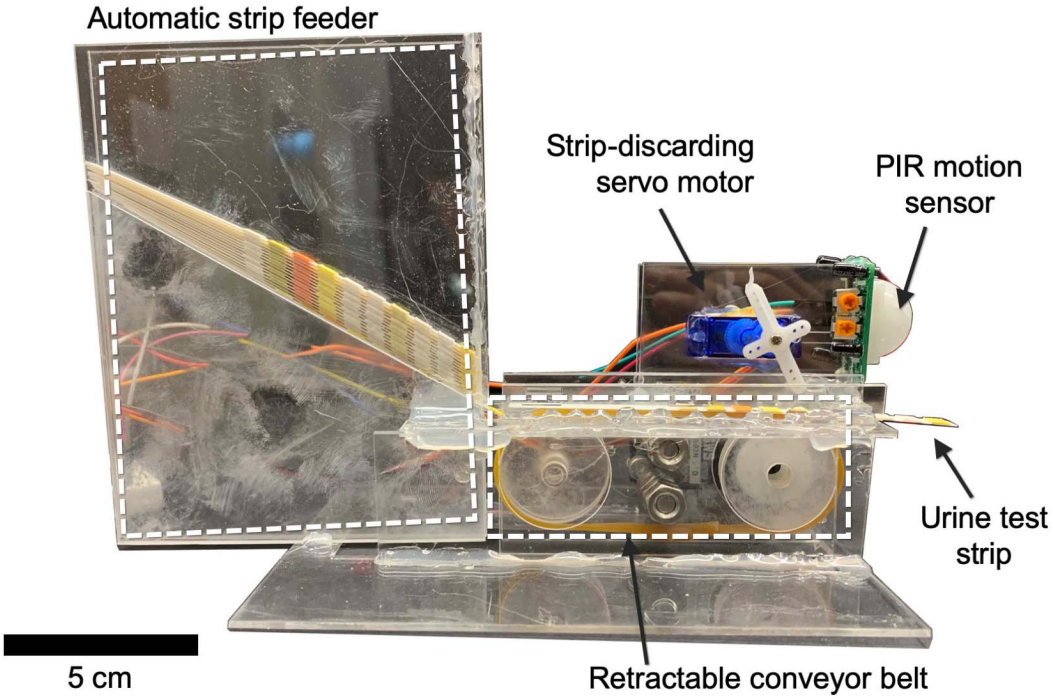

Supplementary Figure 2. Retractable urinalysis subunit. The retractable urinalysis subunit consists of a PIR motion sensor, an automatic strip feeder, a retractrable conveyor belt, and a strip-discarding servo motor.

For the retractable urinalysis subunit, an automatic strip feeder places a stack of urinalysis strips at an angle so that each strip can slide down to the custom-built retractable conveyor belt. The rubber conveyor belt is controlled by a servo motor (S03N-STD, GSW Tech Co., Taipei, Taiwan) which grabs the strip and rotates in both the clockwise and counter-clockwise directions in order to extend and retract the strip. When the PIR motion sensor (HC-SR501, Adafruit, New York, NY) in the front-most position of

the subunit detects a urine stream, the urine strip extends out so that a user can urinate onto the strip. Once the urination event is done, the conveyor belt retracts the strip for the colorimetric recording (**Supplementary Figure 3**). After the colorimetric recording is completed, the conveyor belt extends the strip out and the strip-discarding servo motor (MS-R.1.3.9, Olimex Ltd., Plovdiv, Bulgaria) pushes it into the toilet bowl.

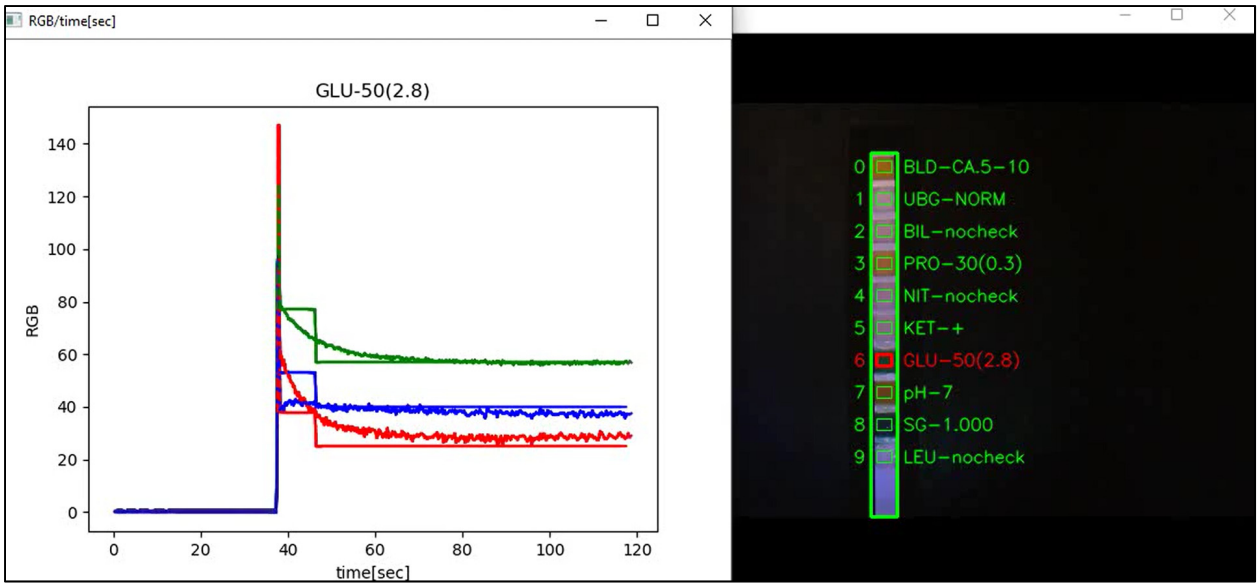

Supplementary Figure 3. A real-time graphic user interface (GUI) that plots RGB kinematics for monitoring the color change of the urinalysis strip.

A separate subunit was developed for real-time colorimetric recording. The subunit consists of a dark box (¼" acrylic sheet) with a camera (Raspberry Pi Camera Module v2, Raspberry Pi Foundation, Cambridge, UK) on the top and a strip entrance at the bottom (**Supplementary Figure 3**). The module detects 10 different regions-of-interest (ROIs) corresponding to 10 different chemical pads in real-time as the urinalysis strip appears in the camera field-of-view (FOV). The graphic user interface (GUI) allows the user to select each ROI as it plots a dynamic RGB chart for monitoring the color change of the selected

urine test component (**Supplementary Figure 3**). Regardless of the chosen ROI, the RGB values of all ROIs are recorded in a separate text file.

Dual-camera-based High-frame-rate Uroflowmetry (Computer Vision Uroflowmetry)

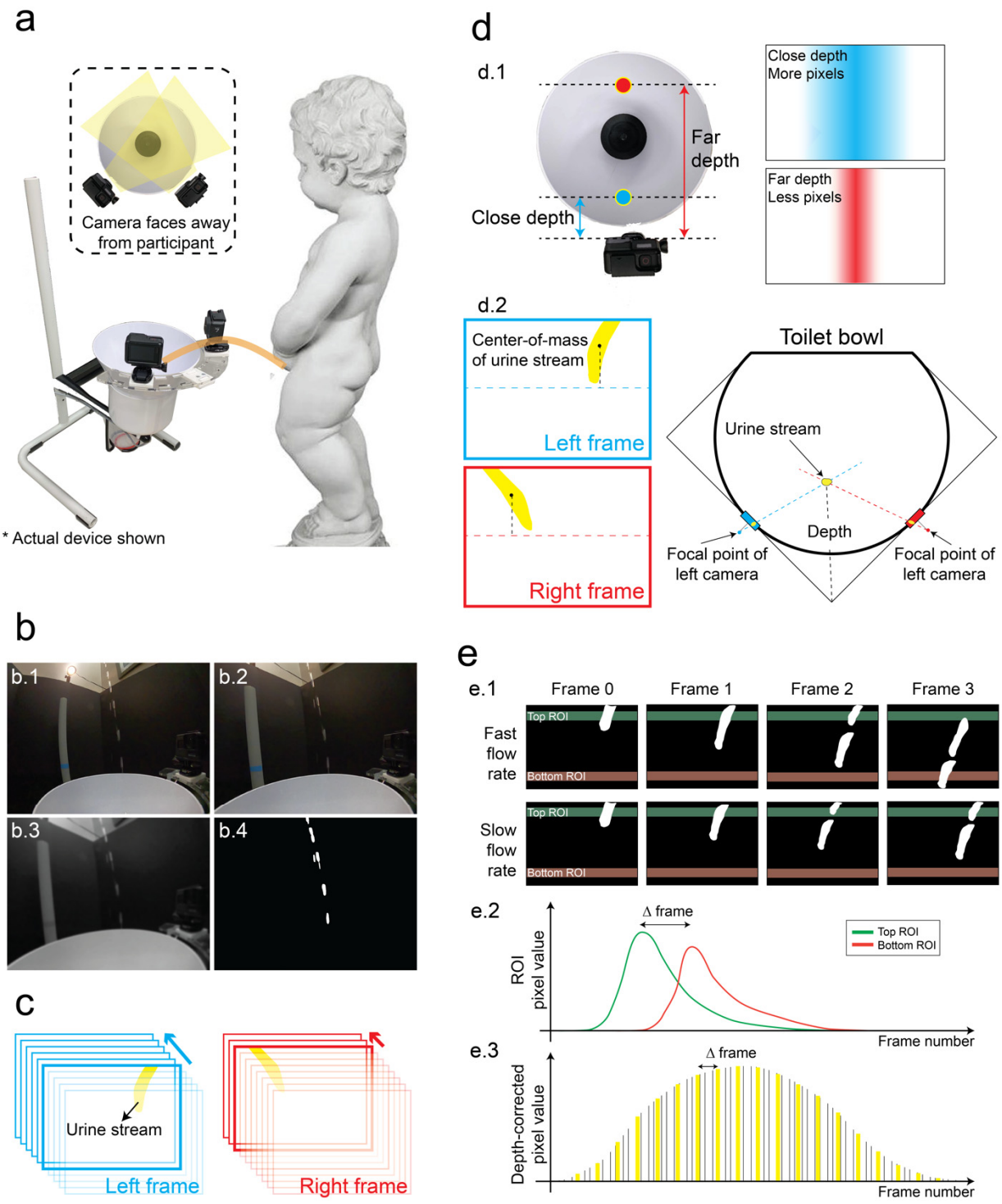

Supplementary Figure 4. Dual-camera-based high-frame-rate uroflowmetry. **a**. Prototype of the camera-based uroflowmetry installed on the standard uroflowmetry. Two GoPro cameras are positioned at the right angle facing away from the user in order to capture and analyze the physical properties of the urine stream. **b**. Image preprocessing step of a urination frame from a participant: (b.1) raw capture of a urine stream falling into the wide angle camera FOV, (b.2) undistortion of the wide angle FOV frame, (b.3) black and white conversion and smoothing, (b.4) a background subtracted frame only extracting the urine stream. **c**. Synchronization of left and right camera frames. **d**. Depth estimation (shown in the schematic) (d.1) Limitation of a single-camera because of the lack of depth information, (d.2) Depth-estimation from two synchronized frames using the geometric calculation. **e**. Flow rate-estimation and correction (shown in the schematic) (e.1) Erroneous measurement of the urine volume from varying flow rates, (e.2) Flow rate-estimation using two ROIs within the camera frame, (e.3) Flow rate-correction is performed by dividing the total sum of the depth-corrected pixel values by the frame shift.

Setup

We have developed a camera-based uroflowmetry module consisting of two high-frame-rate video-recording cameras (GoPro Hero7, GoPro Inc., San Mateo, CA). Multiple iterations of prototypes were developed to correct for several parameters which will be described below. As the camera-based uroflowmetry analyzes the urine stream captured into a series of frames, (1) the depth (the distance of the stream from the camera) and (2) the flow rate of the urine stream could provide erroneous results. For these reasons, two GoPro Hero7 cameras (240 fps [frames-per-second]), 960 × 1280 resolution, wide angle FOV) were positioned at the right angle (**Supplementary Figure 4a**). Detailed analysis steps are described below.

Analysis

All of the image analysis was performed using Python 3.7 on MPEG-4 Part 14 (MP4) video files.

1. Image preprocess

From each left and right camera, the video file (MP4) was imported as a series of frames. For only extracting the urine stream component, each frame was preprocessed by (a) undistortion of the fisheye effect, (b) black-and-white conversion, (c) smoothing, and (d) background removal (**Supplementary Figure 4b**). The GoPro at its maximum frame rate (e.g., 240 Hz) only allows the wide angle FOV instead of the standard linear FOV. The wide angle FOV captures the frame with a fisheye effect which shows radial and tangential distortions. The calibration matrix determining the distortion parameters was acquired using a chess board calibration grid, then implemented as an undistortion matrix for removing the fisheye effect from each frame (**Supplementary Figure 4b**). After the undistortion, each RGB color frame was converted to black-and-white frames and smoothed using the Gaussian blur function (gaussian kernel size: 31) (**Supplementary Figure 4b**). Then, series of frames were fed into background removal function for only extracting the urine streams (**Supplementary Figure 4b**).

2. Synchronization

The recordings of the two cameras initiated manually; therefore, the frames from the left and right cameras were not precisely synchronized. As a result, the synchronization process was performed to correctly align the left and right frames. While iterating through the initial frames, the frame that consisted of the first urine drop motion was detected using a threshold from both left and right frames. Once the first frames from each camera were detected, all earlier frames were removed and the two cameras were successfully synchronized (**Supplementary Figure 4c**).

3. Depth-estimation/correction

A single camera cannot capture the urine stream volume accurately as it lacks the depth (distance from the camera) information (**Supplementary Figure 4d**). Varying depth of the urine stream could result in erroneous measurement of an accurate volume. As such, the depth-corrected urine volume was estimated through geometric calculation using two cameras positioned at a right angle (**Supplementary Figure 4a**). From the synchronized frames, the centers-of-mass of the urine pixels are calculated for each left and right frame. Since the exact positions of the camera and their relative focal points are known, the depth of the urine stream was estimated through trigonometric equations (**Supplementary Figure 4d**). Once the depth was estimated, the depth-corrected pixel value was derived via the equation below.

$$Depth\ corrected\ pixel = Depth\ \times \sqrt{Pixel_{Left}^2 + Pixel_{Right}^2}$$

4. Flow rate-estimation/correction

In addition to the depth effect, varying flow rates of the urine stream can lead to miscalculation of the urine volume (**Supplementary Figure 4e**). With a fixed camera frame rate, more frames of the urine stream will be captured when the urine flow rate is slower as compared to the urine stream with a higher flow rate. To estimate the flow rate of the urine stream, two regions-of-interest (ROIs) were selected in each frame; the top ROI and the bottom ROI (**Supplementary Figure 4e**), where each vertically covered 10% of the frame pixels. The pixel values in those two ROIs were recorded and fed into cross-correlation function for measuring the similarity of two series by outputting the displacement of one relative to the other (**Supplementary Figure 4e and 4e**). Thus, the cross-correlation outputs the number of frames counted for the urine stream to fall from

the top ROI to the bottom ROI. This frame shift (∆f) indicating the number of frames, for which a certain urine drop repeatedly counted, then inversely corresponds to the flow rate of the urine stream. Therefore, to correct for the estimated flow rate, the total sum of the depth-corrected pixel values was divided by the average frame shift between left and right cameras as shown in the equation below (**Supplementary Figure 4e**).

$$Volume \propto \frac{\sum Depth\ corrected\ pixel}{(\Delta f_{Left} + \Delta f_{Right})/2}$$

In order to capture multiple frames of the falling stream, the camera was running at its maximum frame rate of 240 fps.

Accuracy of Multiclass Classification

Briefly, assuming a classification problem with S, samples $S = \{s_i : 1 \leq i \leq S\}$ and *N* classes $\{1, \ldots, N\}$, two functions called true class $\mathrm{tc}(s)$ its predicted class $\mathrm{pc}(s)$ (or True Class II in our study) that map $S \to \{1, \ldots, N\}$ can be defined. Thus, the corresponding confusion matrix becomes a square matrix $C \in \mathcal{M}\{(N \times N, \mathbb{N})$, in which *ij*-th entry C_{ij} is the number of elements of true class *i* that have been assigned to class *j* by the classifier:

$$C_{ij} = |\{s \in S : \mathrm{tc}(s) = i \;\&\; \mathrm{pc}(s) = j\}|$$

The accuracy of a given confusion matrix is defined as the ratio of the correctly classified samples overall.

$$\mathrm{Accuracy} = \frac{\sum_{k=1}^{N} C_{kk}}{S} = \frac{\sum_{k=1}^{N} C_{kk}}{\sum_{i,j=1}^{N} C_{ij}}$$

In our study, we can have two physicians' classifications serve as true classes. Thus, we define this value, "accuracy" as "match rate". The two physicians' classification match rate is 74.89% and the kappa value of these two classification according to Landis *et al*[24]. is 0.655 as shown in **Supplementary Table 3**. If this task was reduced to only a 3 class classification (comprised of "constipated", "normal" and "diarrhoea"), the "match rate" would increase to 0.90.

Supplementary Table 3. The confusion matrix between two physicians' classification.

Physician A Classification	Physician B Classification I	II	III	IV	V	VI	VII		Accuracy
I	11	0	0	0	0	0	0	11	100%
II	9	40	0	0	0	0	0	49	81.63%
III	1	114	205	21	5	0	0	346	59.25%
IV	1	27	186	836	52	0	0	1102	75.86%
V	1	1	4	74	383	19	0	482	79.46%
VI	0	3	1	6	57	271	4	342	79.24%
VII	0	0	0	0	0	7	23	30	76.67%
	23	185	396	937	497	297	27	2362	
Accuracy	47.83%	21.62%	51.77%	89.22%	77.06%	91.25%	85.19%		

Matthews Correlation Coefficient (MCC).

The MCC was introduced by biochemist Brian W. Matthews in 1975[25] and has served as a measure of the quality of binary classifications. Its expansion to multiclass classification was introduced in reference[26]. The following main concept of MCC was introduced in the previous literature[27]. In sum, let $X, Y \in \mathcal{M}(S \times N, \mathbb{F}_2)$ be two matrices where $X_{\mathrm{sn}} = 1$ if the sample s is predicted to belong to class $n(\mathrm{pc}(s) = n)$ and $X_{\mathrm{sn}} = 0$ elsewhere. The same goes to Y_{sn}. With Kronecker's delta function, these can be defined as the following equation.

$$X = (\delta_{\mathrm{pc}(s),n})_{sn} \qquad Y = (\delta_{\mathrm{tc}(s),n})_{sn}$$

The covariance function, a measure of how much two variables change together, between the two can be defined as the following:

$$\mathrm{cov}(X, Y) = \frac{1}{N}\sum_{s=1}^{S}\sum_{k=1}^{N}(X_{sk} - \bar{X}_k)(Y_{sk} - \bar{Y}_k)$$

The MCC is defined in the following equation:

$$\mathrm{MCC} = \frac{\mathrm{cov}(X,Y)}{\sqrt{\mathrm{cov}(X,X)\mathrm{cov}(Y,Y)}}$$

$$= \frac{\sum_{k,l,m=1}^{N} C_{kk}C_{ml} - C_{lk}C_{km}}{\sqrt{\sum_{k=1}^{N}\left[\left(\sum_{l=1}^{N} C_{lk}\right)\left(\sum_{f,g=1,f\neq g}^{N} C_{gf}\right)\right]}\sqrt{\sum_{k=1}^{N}\left[\left(\sum_{l=1}^{N} C_{kl}\right)\left(\sum_{f,g=1,f\neq g}^{N} C_{fg}\right)\right]}}$$

The MCC ranges from -1 to 1, where -1 indicates completely disordered classification and 1 indicates perfect classification. The MCC between the two physicians is determined to be 0.70.

Confusion Entropy (CEN).

According to previously published literature[26-28], the entropy of the classification, H is defined to be the expected value of the self-information $I(x) = -\log p(X)$ with a random variable X.

$$H(x) = \sum_{x\in X} p(x)I(x) = \sum_{x\in X} p(x)\log p(x) = \sum_{x\in X} h_b(x)$$

where $p(x)$ denotes the probability mass function of X.

The CEN for a confusion matrix C can be defined as follows:

$$\mathrm{CEN} = \sum_{i=1}^{N} P_i \mathrm{CEN}_i = \sum_{i=1}^{N} P_i \sum_{j=1,j\neq k}^{N} h_{2(N-1)}\left(P_{ij}^{i}\right) + h_{2(N-1)}\left(P_{ji}^{i}\right)$$

$$= \sum_{i=1}^{N} \frac{\sum_{j=1}^{N}(C_{ij}+C_{ji})}{2\sum_{j,k=1}^{N} C_{jk}} \sum_{j=1,j\neq k}^{N} h_{2(N-1)}\left(\frac{C_{ij}}{\sum_{k=1}^{N}(C_{ik}+C_{ki})}\right) + h_{2(N-1)}\left(\frac{C_{ij}}{\sum_{k=1}^{N}\left(C_{jk}+C_{kj}\right)}\right)$$

In our study, we have four (toilet status) or seven classes (BSFS) ($N > 2$). Thus, this measure lives in the range [0, 1] where 0 stands for perfect classification and 1 for the completely disordered classification. The CEN value of our study is 0.25.

a Receiver Operating Characteristics – Training Set, Physician A

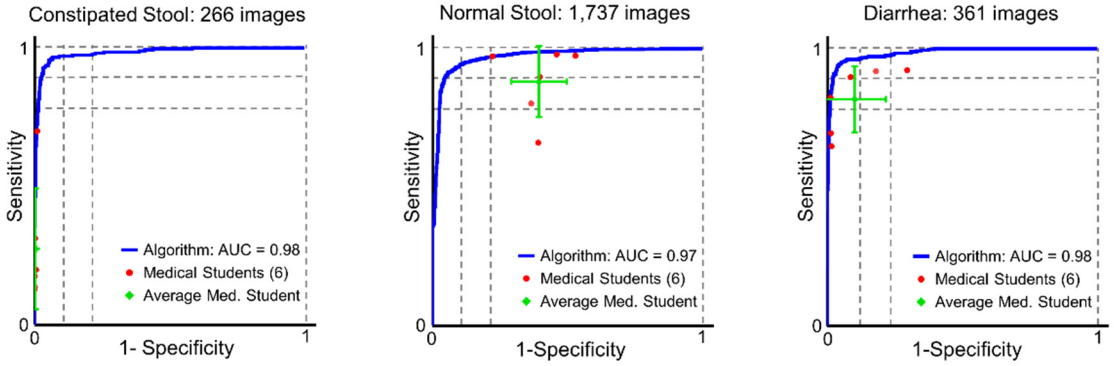

b Receiver Operating Characteristics – Test Set, Physician A

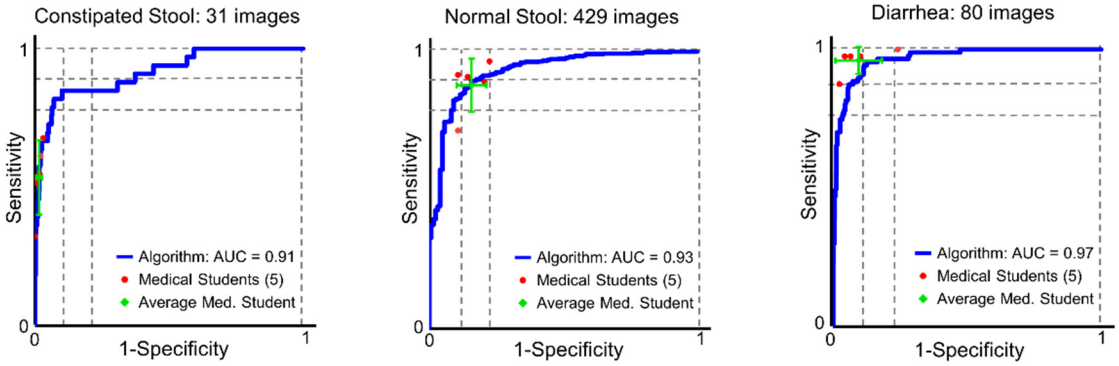

c Receiver Operating Characteristics – Training Set, Physician B

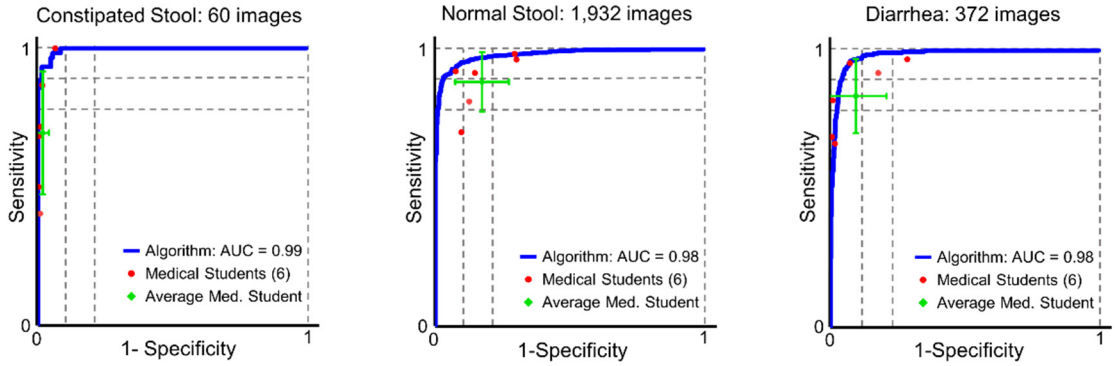

d Receiver Operating Characteristics – Test Set, Physician B

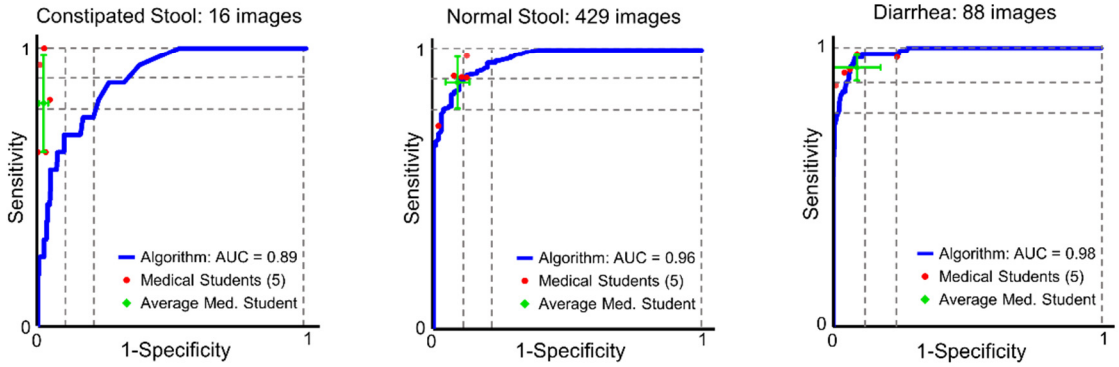

Supplementary Figure 5. Stool classification performance of the algorithm versus medical students. Six medical students (training sets) and five medical students (test sets) produced a single prediction per image, represented by single red points. Averages and standard deviations of the medical students for each task were represented by green points, lines, and caps. **a.** The classification task here is reduced to a trichotomous task spanning constipation, normal stool and diarrhoea, based on the stool taxonomy shown in **Figure 3c**. Corresponding receiver operator characteristics (ROCs) were generated on a basis of a ground truth by physician A. The deep learning convolutional neural network (CNN) outperformed the average of untrained medical students when using the training set of stool images, indicating the algorithm follows board-certified surgeons' decision with high accuracy. All area under curves (AUCs) were greater than 0.97. These ROCs were generated on a basis of a multiclass classification strategy, the one-vs.-rest. **b.** When using a completely new stool image set, the CNN provided comparable accuracy with those of trained medical students. All area under curves were greater than 0.91. **c.** Similar ROCs were generated, based on physician B's classification as a ground truth. Similarly, the deep CNN showed higher accuracy in the test set than those of untrained medical students. All ROCs showed extremely high AUCs, which are all greater than 0.98. d. Similar patterns were observed when using the new stool image set with the ground truth provided by physician B. The CNN demonstrated comparable accuracy with those of trained medical students.

Smart Phone Stool Analysis

We also deployed many of the features described in the main section using a smartphone for users without access to a Smart Toilet for stool analysis. We created an iOS-based application by transferring our retrained tensors, the information obtained when training our CNN, from a laptop with the Inception v3 architecture to a mobile device. We used the Core ML framework released by Apple Inc., which allows developers to integrate machine learning into their iOS applications. The application was created with Xcode (Apple Inc., Cupertino, CA, USA), an integrated development environment for macOS. The current version of the application allows users to upload a stool image acquired by the users and the transferred tensors classify the stool accordingly. The developer tool we employed in this manuscript is Xcode Version 11.2 (11B52). The application was emulated and tested with iPhone 11 Pro Max, iPhone 11 Pro, iPhone 11,

iPhone X, iPhone XR, iPhone XS, iPhone 8 Plus, iPhone 8, iPhone 7 Plus, iPhone 7, iPad Pro (12.9-inch) (3rd generation), iPad Pro (11-inch), iPad Pro (9.7-inch), iPad Air (3rd generation), and iPad (7th generation). In the future application, embedded user identification methods such as facial recognition and fingerprint sensor (TouchID) in the smart phone will annotate generated data with the appropriate user and securely transfer the annotate data to a cloud system. We expect this mobile application will greatly extend the reach of our technology even in the absence of an in-home toilet system.

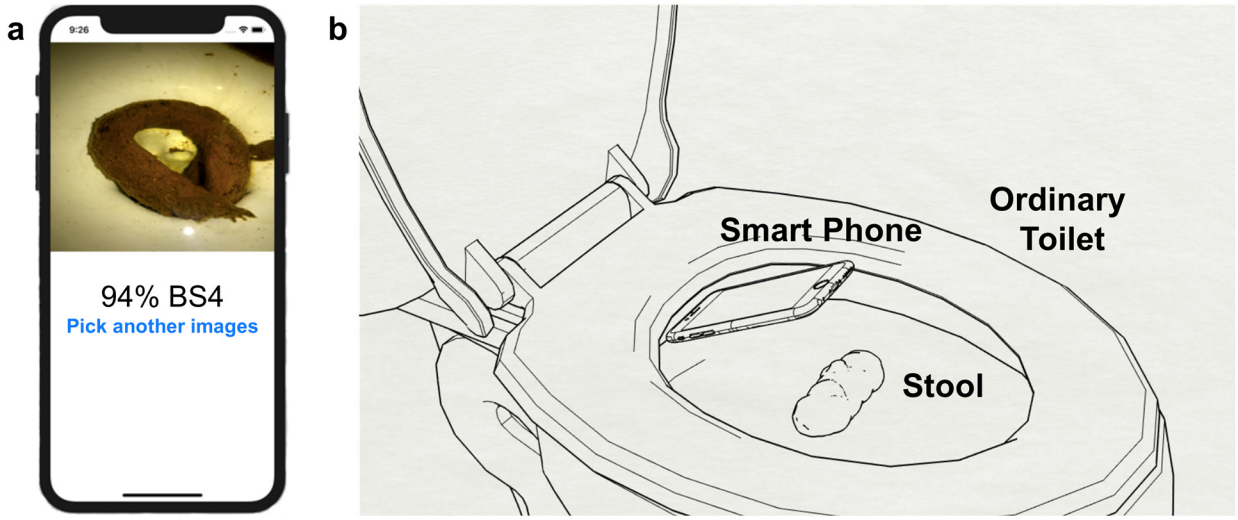

Supplementary Figure 6. Smart phone stool analysis. **a**. The mobile application interface is shown. This enables users to upload a stool image for the machine learning application. The image is then classified automatically. **b**. In an ordinary toilet environment, users are instructed to take a photo of stool with their own mobile phone.

Measures of Image Similarity

To gadget an additional biometric identification process in the toilet system, a new identification module that recognizes a user's pattern of anal creases (so-called "analprint") was implemented. The aim of the biometric identification process is to match the acquired images/videos by the system with stored reference data to provide reliable/reproducible recognition of a person's identity. A universal serial bus (USB) camera attached to a microprocessor (Raspberry Pi) acquires video stream on the region of interest (i.e. anus or anoderm) when a seating signal from the pressure sensor is detected. Then, three algorithms are employed to compare the fragmented frames with the reference frames stored in the system—the mean squared error (MSE), the Structural Similarity Index Measure (SSIM), and a deep convolutional neural network (CNN). A measure of MSE between two images $g(x, y)$ and $\hat{g}(x, y)$ is:

$$\mathrm{MSE} = \frac{1}{MN}\sum_{n=1}^{M}\sum_{m=1}^{N}[\hat{g}(n,m) - g(n,m)]^2$$

This equation averages the squared intensity differences of acquired and reference image pixels. A value of 0 for MSE indicates perfect similarity, while a value greater than 100 implies less similarity and will continue to grow as the average difference between pixel intensities increases as well. In practical use, however, the MSE is flawed as often times images of the same subject will have dramatically different pixel values, for example, when taken under different lighting conditions, leading to large MSE values.

While the MSE measures the perceived errors from pixels, the SSIM estimates the perceived change in the structural information of the image and often provides greater

insights. Wang *et al*. introduced this framework to improve image comparison by fixing some of issues related with MSE. This structural similarity index is defined as below:

$$\mathrm{SSIM}(x,y) = \frac{(2\mu_x\mu_y + c_1)(2\sigma_{xy} + c_2)}{(\mu_x^2 + \mu_y^2 + c_1)(\sigma_x^2 + \sigma_y^2 + c_2)}$$

where μ_x stands for the mean intensity,

$$\mu_x = \frac{1}{N}\sum_{i=0}^{N} x_i$$

while σ_x indicates the standard deviation (the square root of variance) as an estimate of the signal contrast.

$$\sigma_x = \sqrt{\frac{1}{N-1}\sum_{i=1}^{N}(x_i - \mu_x)^2}$$

whereas $c_1$and c_2 are constants to avoid instability when $\mu_x^2 + \mu_y^2$ approaches to zero.

The third method of measurement uses a CNN to classify the stool in the previous section. Since modern image recognition necessitates millions of parameters, model training from scratch requires much more computational power with a large amount of data that is already labelled with a classification. To most efficiently approach this problem, we employed transfer learning, a method in which a CNN that has been rigorously trained on other related data can be applied to a new problem by only retraining a small portion of it. In our case we use a transfer learning methodology with TensorFlow (Google Inc.) to recycle feature extraction capabilities from a powerful image classifier[29] (InceptionV3) trained on ImageNet and then simply retrain the penultimate layer of the network.

In order to use all the algorithms to determine the identity of a user via their analprint, we must compare a user's analprint at the time of toileting to a reference set of analprints for all possible users. When the current user's print is compared to the references, the lowest MSE-scoring reference analprint will identify the user. In our case we calculate the MSE scores for each frame in the video taken, and then take the average. For example, consider a single participant. For research participant 1, the MSE value between their current analprint and their corresponding participant 1 reference print is 184, while the lowest MSE value of any other participant when comparing to the participant 1 reference analprint is 612. Since the lowest MSE identifies the best match, this method correctly identifies participant 1. Furthermore, the SSIM value between the test set (Participant #1's current analprint) and the reference set (Participant #1's reference analprint) is averaged to be 0.79, while MSE values of the remaining participants (their test sets vs. participant 1's reference print) were lower than 0.72, also correctly identifying that participant 1 is the best match. Finally, the CNN prediction was 88 ± 22.17% (all frames averaged) while all other participant's CNN predictions were never higher than 9.2%. All other comparisons were detailed in the **Supplementary Table 4**. As can be seen in **Supplementary Table 4**, in most cases, all algorithms provide a reasonable distinction of the research participant by analysing the pattern of the anus. In addition, we believe that acquiring the entire defecation process from the anus will facilitate not only reliable recognition of a person's identity, but also accurate measure of the amount of excreta and diagnosis of certain medical symptoms such as haemorrhoids. All data including images, videos, and user information generated by the toilet system were stored in an online, shared folder. This folder was shared with the host server

performing machine learning and user annotations on the generated dataset. After uploading, remaining datasets in a local machine were deleted to protect user's privacy.

Supplementary Table 4. Comparison between the test sets from the participants and the stored reference sets via the mean squared error (MSE), the structural similarity indices (SSIM) and the deep convolutional neural network (CNN).

			Reference Sets									
			P1	**P2**	**P3**	**P4**	**P5**	**P6**	**P7**	**P8**	**P9**	**P10**
Test Sets	**P1**	MSE	**184.27**	877.83	1126.2	2838.1	809.72	3404	2919.2	1905.8	1805.1	612.58
		SSIM	**0.79**	0.72	0.56	0.56	0.63	0.53	0.53	0.57	0.52	0.63
		CNN	**0.89**	0	0.09	0.01	0	0	0	0	0	0
	P3	MSE	1338.9	410.44	**387.54**	1264.7	793.92	1076.2	1434.7	605.12	810.51	1282.4
		SSIM	0.6	0.62	**0.64**	0.48	0.57	0.53	0.5	0.55	0.46	0.49
		CNN	0	0	**1**	0	0	0	0	0	0	0
	P4	MSE	3116.5	1218.6	1777	**203.81**	1276.8	446.82	1274.4	540.9	920.52	2779.8
		SSIM	0.53	0.6	0.51	0.6	0.54	0.61	0.53	0.56	0.53	0.46
		CNN	0	0	0	**0.93**	0	0	0	0.05	0.01	0
	P5	MSE	964.88	874.77	1150.7	2126.3	**385.81**	2385.9	2036.8	1273	1499	907.14
		SSIM	0.61	0.6	0.52	0.45	**0.69**	0.49	0.47	0.52	0.44	0.51
		CNN	0.02	0.03	0.03	0	**0.56**	0.01	0	0.02	0.09	0.23
	P6	MSE	1792.8	559.2	1050.1	832.43	658.72	**478.64**	1518.7	556.35	521.9	1490.3
		SSIM	0.62	0.67	0.56	0.54	0.61	0.66	0.53	0.59	0.54	0.52
		CNN	0.03	0.02	0	0.02	0	**0.9**	0	0.02	0	0
	P8	MSE	2979.2	1289.9	1780	380.6	944.39	350.96	1392.5	**262.47**	805.03	2600.3
		SSIM	0.53	0.56	0.48	0.53	0.55	0.61	0.5	**0.64**	0.51	0.45
		CNN	0	0	0	0.01	0	0	0	**0.98**	0	0
	P10	MSE	764.2	1429.2	1614.9	3991.1	1832.9	3969.9	3969.9	2906.5	2585.9	**672.06**
		SSIM	0.66	0.61	0.55	0.42	0.57	0.45	0.45	0.47	0.43	**0.64**
		CNN	0	0	0	0.01	0.02	0.01	0.02	0	0.04	**0.91**

Smart Toilet User Acceptance Survey

To assess the user acceptance of the Smart Toilet (this is the exact wording used in the actual survey), we have created and distributed a “Smart Toilet User Acceptance Survey,” which is approved by the Stanford IRB (protocol number: 51666). The survey briefly introduces the main concept of Precision Health and describes relevant functionalities of the Smart Toilet. After the introduction, the survey asks the users’ acceptance and compliance to potentially sensitive features of the Smart Toilet. A total of 300 surveys were recorded from the Stanford community. We acknowledge that this population does not fully represent the general public; however, we were able to draw some interesting results from this survey.

Demography

Questionnaires were distributed to Stanford-affiliated email lists. Altogether, 300 questionnaires were returned and analysed. Questionnaires broached issues regarding Precision Health and Smart Toilet related information (e.g., user acceptance per Smart Toilet module, compliance, awareness of new biometric identifiers) and on some basic sociodemographics. Since a toileting event is very gender-sensitive, all individual responses were categorized by gender. In this survey, 153 participants identified themselves as “Male”, while 135 identified as “Female”. It should be noted that the survey offered non-binary gender options as well, and 12 identified as “Other” or recorded no response. Moreover, it is important to mention that the majority of survey responses (43.67%) were from individuals with doctoral or professional degrees. The full demographic information of the survey participants is shown in **Supplementary Figure 7**. We note that our survey population is biased because it represents a highly educated

group from one geographic location, which may systematically over- or under-estimate population preferences toward the Smart Toilet.

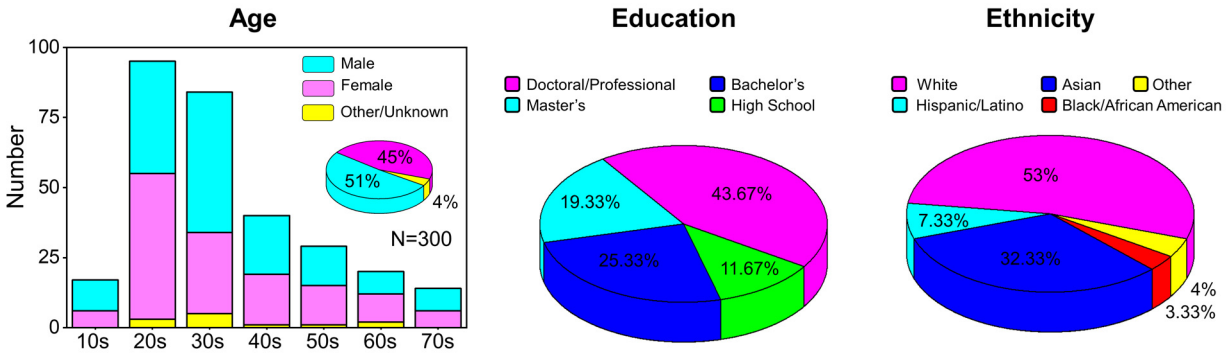

Supplementary Figure 7. Smart Toilet User Acceptance Survey: Demography

Compliance

Since we first began developing the Smart Toilet, we have designed the system to minimize any human behaviour/intervention required for the system's operation. This feature is also very important for potential users as the majority of survey participants responded that "minimizing human intervention (not interfering with normal human behaviour)" is either very important (49.49%) or somewhat important (36.79%). Specifically, fifteen survey respondents emphasized this feature. Since this design consideration has been our top priority throughout the development of the Smart Toilet, we expect to see high overall user compliance of the Smart Toilet system.

Acceptance

The overall acceptance of the Smart Toilet system as well as participants' acceptance level per module are shown below in **Supplementary Figure 8**. A 5-point Likert scale was employed in order to assess the different factors that could potentially

elevate or depress users' comfort levels towards Smart Toilet technologies. Interestingly, we observed a statistically significant preference of non-camera based modules (the urinalysis and fingerprint modules over uroflowmetry, stool analysis and analprint modules combined, $p < 0.0001$, two-sample t-test). The most accepted module is urinalysis while the least favoured module is analprint. After explaining each respective module to the participant, we asked him or her the overall acceptance of the Smart Toilet system. We noted that the overall acceptance level of the Smart Toilet system is within an acceptable range as the majority of responses were either "somewhat comfortable" (37.33%) or "very comfortable" (15.33%) to use the Smart Toilet system. More than half of the respondents (52.67%) feel that the system is comfortable to use in some degree, while 30.00% of the respondents feel uncomfortableness to use (7.33% and 22.67% feel "extremely uncomfortable" and "somewhat uncomfortable", respectively).

As the gender issue is crucial, all responses per individual module with overall Smart Toilet acceptance rates were compared by gender. Owing to the small number ($n = 12$) of respondents from other/unknown genders, the other/unknown genders were excluded from comparison. A gender difference was observed in a camera based module of the Smart Toilet system with a p-value of 0.04 (stool analysis, at 0.05 level). Males are more favourable to this camera-based Smart Toilet modules. Other than this module, gender differences were not observed with large p-values of 0.53 (overall acceptance), 0.22 (urinalysis), 0.06 (uroflowmetry), 0.67 (fingerprint) and 0.27 (analprint).

In order to avoid any potential framing effect, we directly asked the survey participants the following questions. "Would you feel comfortable with a camera in the toilet bowl that captures stool images and pictures of your anus?". 35.67% of the

respondents answered “YES” while the remaining individuals (64.33%) answered “NO”. We asked again, “Would you be comfortable with a camera in the toilet bowl that ONLY captures stool images and does not take pictures of your anus?”. 75.33% of the respondents answered “YES”, while the rest of the participants (24.67%) answered “NO”. Lastly, we asked those who answered “YES” to the question above the following question: “Would you be more comfortable with a "scanner" such as a barcode scanner, instead of a "camera' in the toilet bowl?”. 70.27% of the selected respondents answered “YES”. This result implies that there is a general sense of elevated levels of malaise and apprehension of any cameras taking optical images of the body and excretion.

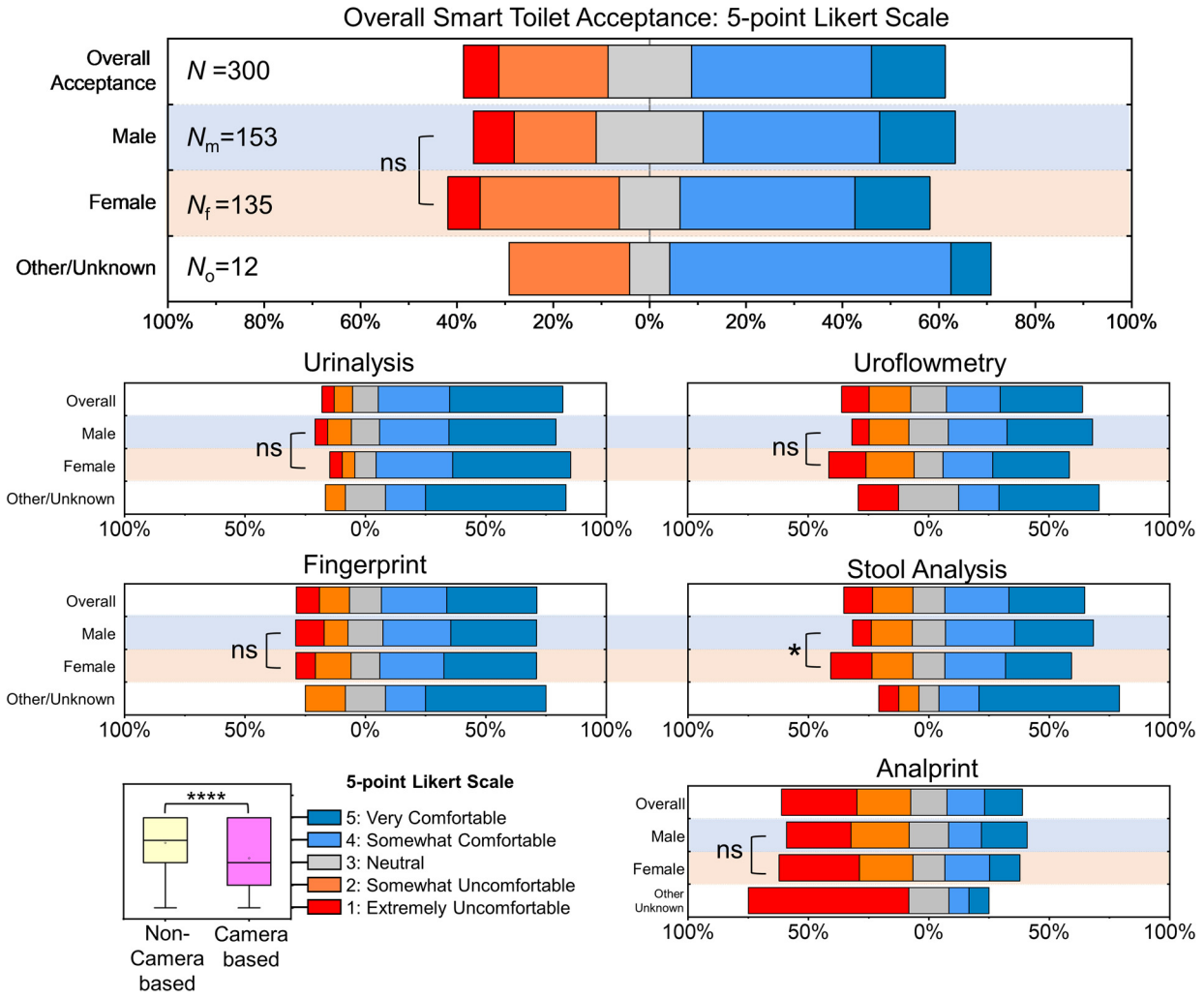

Supplementary Figure 8. The Overall User Acceptance of the Smart Toilet System. Detailed user acceptance levels per Smart Toilet modules are also displayed. No gender-based differences were observed except for the defecation monitoring module (Stool Analysis). Interestingly, the survey participants are more favourable toward using non-camera based assays in the Smart Toilet system (*: *p*-value is less than 0.05 and ****: *p*-value is less than 0.0001).

Correlation

In our survey, no socio-demographical (gender, education and ethnicity) background affects user's acceptance level of the Smart Toilet system. 59.67% of the survey participants responded that they have heard of the concept of "Precision Health". Among them, only 56.98% recognized the difference between "Precision Health" and "Precision Medicine". However, the awareness of "Precision Health", either vaguely or accurately, does not affect the overall user acceptance of the Smart Toilet system as represented by large *p*-values (0.55 and 0.56, respectively, two-sample *t*-test). 34.33% of the survey participants are currently wearing a health monitoring device and 35.67% of the survey participants already use some kind of Smart Home devices. Those who wear a health monitoring device are not statistically different in their Smart Toilet acceptance levels from those who do not wear ($p = 0.39$, two-sample *t*-test). Interestingly, those who use a Smart Home device are significantly more favourable to the Smart Toilet system than those who do not use any ($p = 0.01$, two-sample *t*-test).

Comments/Suggestions

The vast majority of participants' comments/suggestions (from the 86 comments) are regarding privacy protection and data security enactment in the Smart Toilet system. Most of the users' qualms stem from the Smart Toilet's use of a camera as a sensor. Forty comments were regarding obtaining tangible and immediate health-care benefits

from the Smart Toilet system, best represented by a user's quote - "Very clear benefits that are evidence based". Other comments from nineteen respondents are related to the Smart Toilet's cost and affordability. Eighteen respondents mentioned a self-cleaning feature of the Smart Toilet.

A few respondents proposed to use the system first in a clinical setting such as a doctor's office or a pharmacy to increase its awareness and comfort. Some respondents expressed their concerns on our study's use of intrusive terminology/rhetoric (such as analprint and toilet camera). They proposed us to use alternative, less intrusive terminology such as a generic optical sensor or scanner. Other respondents pointed out the importance of the minimal interference with normal human behaviour. Lastly, we believe one of the comments properly represents the current status of our Smart Toilet system: "The concept sounds uncomfortable right now, but that's because it isn't the norm."

Future survey studies will be conducted with broader coverage of diverse socioeconomic classes, cultural backgrounds, and geographic locations.

Privacy and Security

Stanford's Data Risk Assessment

In order to effectively protect users' privacy and secure all data, the current IRB protocol (eProtocol Number: IRB-45621, titled "Continuous Human Health Monitoring via Routine Urinalysis and Stool Analysis") was assessed by the Stanford's Data Risk Assessment (DRA). The Stanford Information Security Office (ISO) and University Privacy Office (UPO) performed a Data Risk Assessment (DRA), an information security and privacy assessment of "Continuous Human Health Monitoring via Routine Urinalysis

and Stool Analysis Data Risk Assessment" in order to not only identify but also mitigate any risks to Stanford University.

The list issued by the DRA to protect privacy:

1. The Stanford research team will issue Stanford encrypted devices (including the toilet system) to research participants for the purpose of collecting the photographs required for the study.
2. The Stanford research team will build a Research Electronic Data Capture (REDCap) web form to allow participants to upload the photographs required for the study directly to REDCap. REDCap is a browser-based, metadata-driven EDC software solution and workflow methodology for designing clinical and translational research databases.
3. All of the research participant data collected both on-site and off-site will be stored in REDCap or Stanford Medicine Box.
4. The videos and photographs collected on the toilet camera will be immediately transferred to REDCap or Stanford Medicine Box and deleted from the toilet camera. The camera of the toilet system must be stored in a secure area or locked drawer when not in use.

The list issued by the DRA to protect security:

1. The Stanford research team ensures that the endpoint device(s) (mobile devices used to capture the images/videos and the laptops/desktops used to access REDCap or Stanford Medicine Box) complies with Stanford's Minimum-Security Standards (https://minsec.stanford.edu) for endpoints as applicable.
2. The Stanford research team adheres to Stanford's password standards

(https://uit.stanford.edu/service/accounts/passwords/quickguide).

3. The Stanford research team configures all data transfers to enforce the use of secure data transmission protocols (e.g., Transport Layer Security 1.1+).
4. The Stanford research team provides a direct method of transferring data on mobile device(s) to REDCap or Stanford Medicine Box.

Potential Identity Recognition

We envision that prior to the installation/deployment of the toilet system, in a local hospital (in which a cloud server is located), users must consult with designated physicians for toilet use and register their fingerprints and analprints accordingly (with the freedom to opt in/out for analprint scan at any anytime.) This process will ensure electronic health record (EHR) compatibility of any generated data from the toilet System. While seating, the motion detector initiated the anus scanner so that all subsequent events will be annotated with the owner of the anus. This will cover 1) male defecation, 2) female defecation, 3) female urination, and 4) male user seated urination (although modules for 3) and 4) are currently under development). After the completion of a defecation and/or urination event, the fingerprint scanner prompts a user via a green light indicator. When the user flushes, the user's identity obtained from the fingerprint scanner will be compared with that from the analprint scanner. When disparity is observed, the generated data will be flagged for identity mismatch. Both the user(s) and designated clinicians will be notified with this disparity, too.

The aspect of the anus may change over time. Regarding the morphological stability of the anus over time, a few studies have already dealt with this concern, by

describing automatic template update strategies for biometrics. Our biometric ID with a combination of fingerprint and analprint can also implement this technology by constantly adapting and updating any changes in appearance. Furthermore, if a significant change in anus' morphology is observed, this observation can be related to disease detection, such as anal fissure or haemorrhoid, which are detectable by our camera-based or machine learning based approach. Nonetheless, if user acceptance and privacy issues regarding the human anus as a biometric identifier rise, the analprint identification method can always be replaced by some other approaches.

Future Toilet System

The effective incorporation of disease-specific tests in the toilet system will require two significant features: a standardized workflow for biomarker analysis and biomarker selection and discovery. First, a standardized workflow for any given biomarker is required. Biochemical analyses of human excreta in a toilet environment would require bulky and expensive analytical instruments and complex sample preparation modules for downstream analysis. Inevitably, it requires a more expensive and complex biochemical analysis system that may not fit within the dimensions of a toilet. Thus, a sample-to-answer type test is more appropriate in the Smart Toilet system. To implement these types of assays within the Smart Toilet system, standard workflows for biochemical analyses of urine/stool will be developed and incorporated. This workflow includes four sub-processes guided by the Department of Defense (DoD) regarding a point-of-care assay development, which are 1) sample collection and preservation, 2) sample preparation, 3) molecular recognition, amplification, and signal transduction, and 4) system integration.

Second, biomarker selection for any given disease will play a vital role in the test incorporation. As listed in our **Supplementary Table 2**, many disease/other states such as urinary tract infections or pregnancy can be monitored/screened with available biomarkers. Endogenous biomarkers such as human chorionic gonadotropin (hCG), luteinizing hormone (LH) and synthetic biomarkers in the forms of minicircle[30], macrophage[31], and nanoworm[32] are all possible ways in which the toilet may eventually be customized to detect those for serial monitoring. Once biomarkers are fully confirmed and validated, the Smart Toilet may be useful to track these biomarkers from human

excretion. Although the delivery of the above-mentioned agents currently requires intravenous injection, orally deliverable agents will be available in the future, and the reporters could be detected by the toilet. We envision that such strategies will be successively and effectively employed in our future toilet system for testing specific diseases and different cancer types. Although the delivery of the above-mentioned agents currently requires intravenous injection, orally deliverable agents are expected to be available in the future, and the reporters could be detected by the toilet. We envision that such strategies will be successively and effectively employed in our future toilet system for testing specific diseases and different cancer types.

Supplementary Table 5. Initial prototype parts for the toilet system. Note that these prices are based on retail market values. Mass production is not considered and not reflected in this price list. Also note that the authors do not have any financial interests with the listed vendors.

Part	Part number and Manufacturer	Price
Urinalysis Reagent Strips	Accutest URS-10 (100 units), Jant Pharmacal Corp, Encino, CA	$ 18.40
Toilet Body Cover	SmartBidet, Bergenfield, NJ	$ 40.00
Toilet Body Seat	SmartBidet, Bergenfield, NJ	$ 70.00
Raspberry Pi v3 Model B	Raspberry Pi Foundation, Cambridge, UK	$ 35.00
Raspberry Pi Camera Module v2	Raspberry Pi Foundation, Cambridge, UK	$ 45.00
Optical Fingerprint Reader Module	GR2904, FlyFun Company, Shenzhen, China	$ 19.85
Analog-to-Digital Converter (ADC)	MCP3008, MicroChip Technology, Chandler, AZ	$ 2.19
Passive Infrared (PIR) Motion Sensor	HC-SR501, Adafruit, New York, NY	$ 9.95
LED strips	WS2815BK300WP (5 m), Alitove, Shenzhen, China	$ 19.99
GoPro Hero 7	GoPro Inc., San Mateo, CA	$ 329.99
Servo Motor	MS-R.1.3.9, Olimex Ltd., Plovdiv, Bulgaria	$ 27.99
PCB Prototyping	Stanford Prototyping Facility	-
Rapid Prototyping (3D print, Laser cut)	Stanford Product Realization Lab, Stanford Biodesign Collab	-

Printed Circuit Board Layout

a

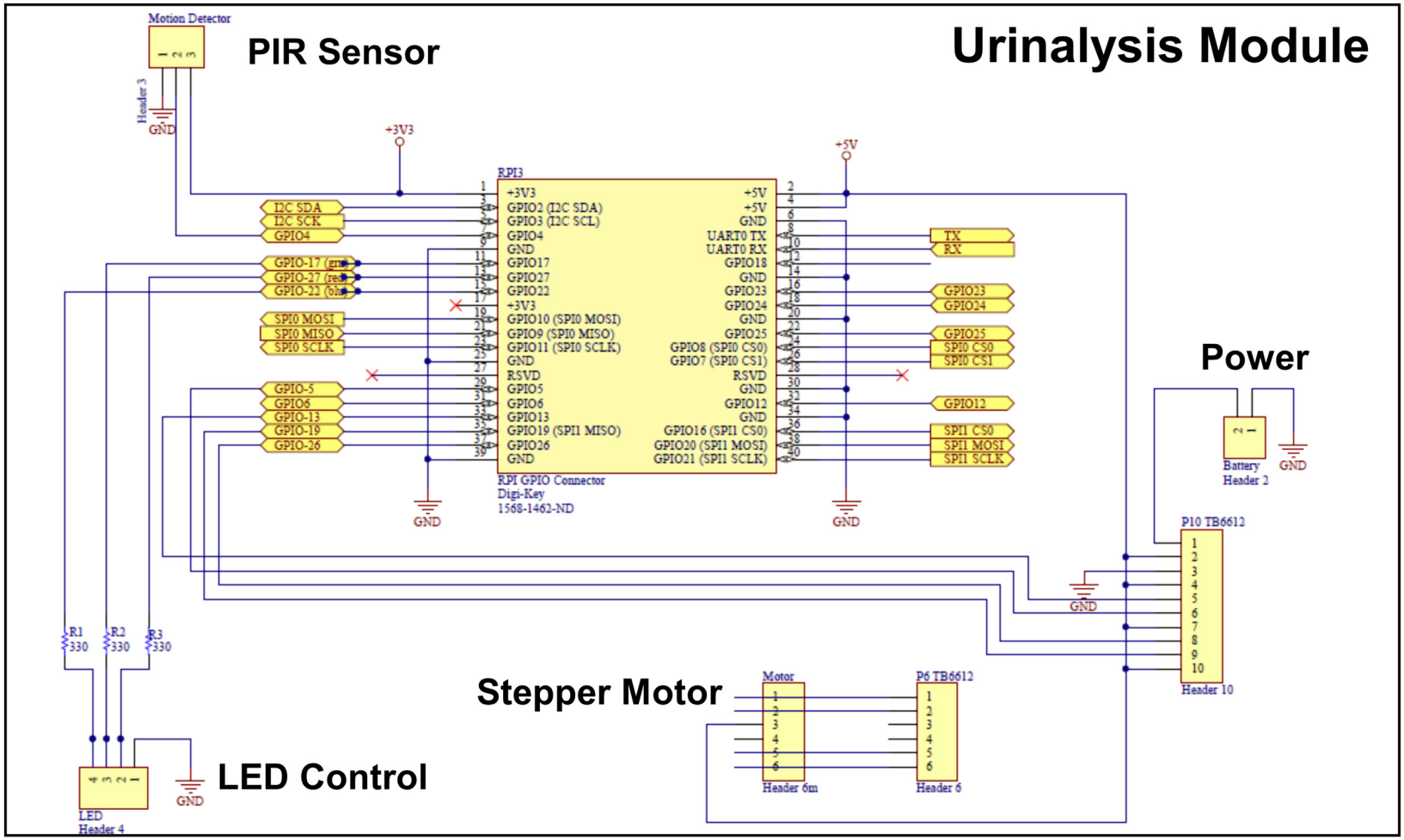

b

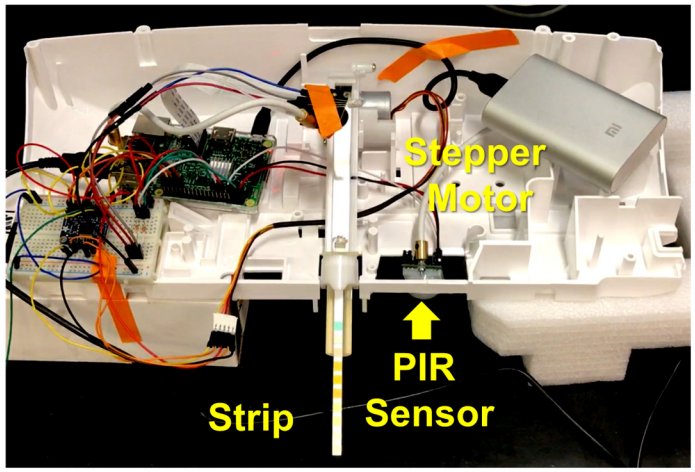
Stepper
Motor
PIR
Sensor
Strip

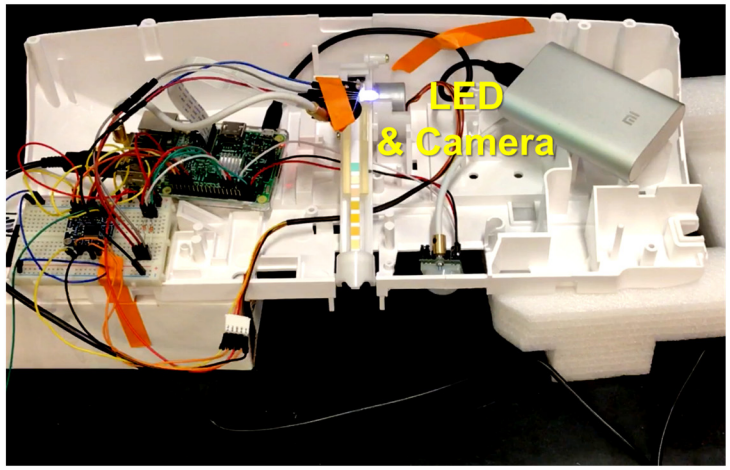
LED
& Camera

c

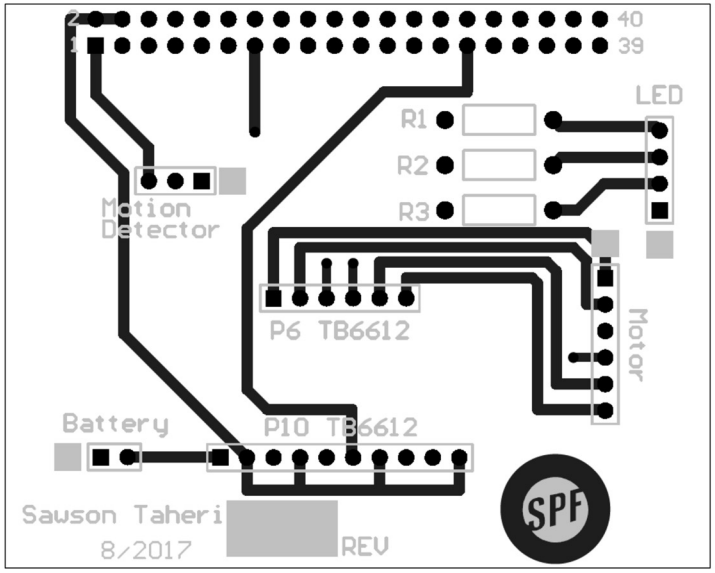
40
39
LED
R1
R2
R3
Motion
Detector
P6 TB6612
Motor
Battery
P10 TB6612
Sawson Taheri
8/2017
REV
SPF

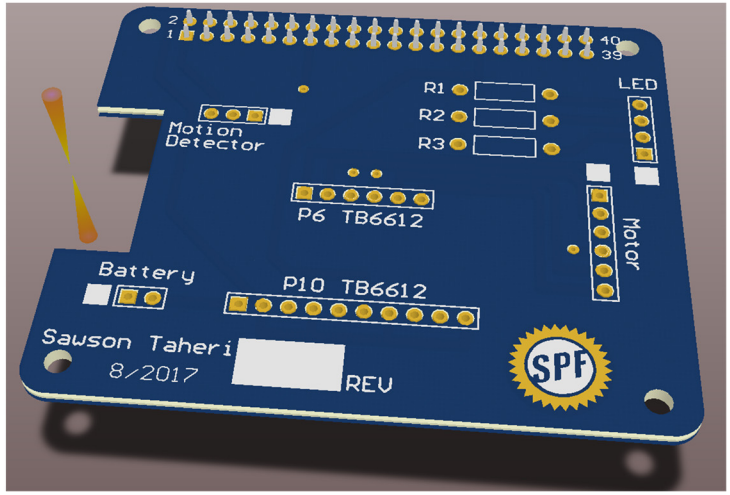
40
39
LED
R1
R2
R3
Motion
Detector
P6 TB6612
Motor
Battery
P10 TB6612
Sawson Taheri
8/2017
REV
SPF

d

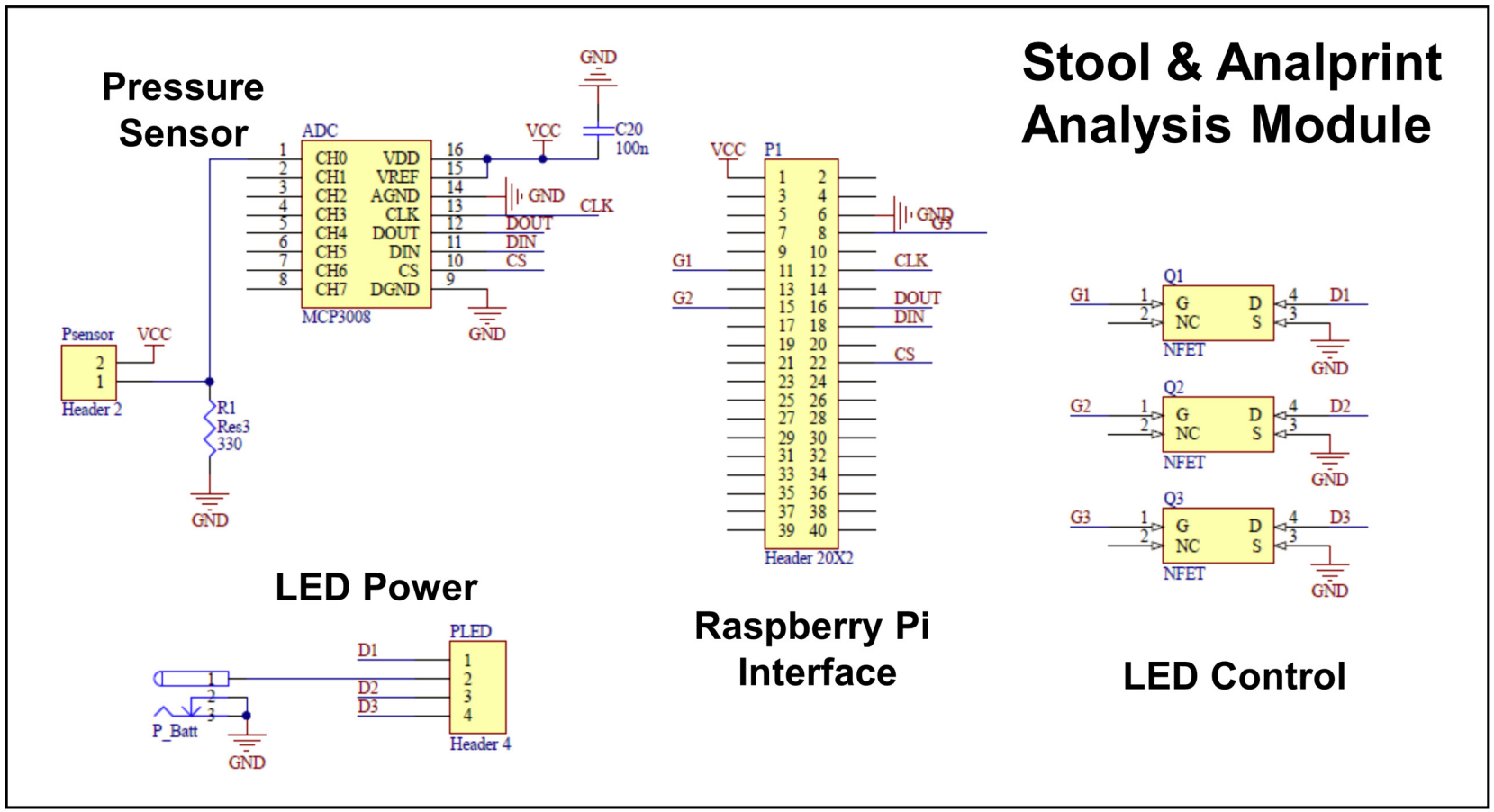
Pressure Sensor
ADC
CH0
CH1
CH2
CH3
CH4
CH5
CH6
CH7
VDD
VREF
AGND
CLK
DOUT
DIN
CS
DGND
MCP3008
GND
VCC
C20
100n
CLK
DOUT
DIN
CS
Psensor
VCC
Header 2
R1
Res3
330
LED Power
PLED
D1
D2
D3
P_Batt
Header 4
P1
Header 20X2
G1
G2
G3
Raspberry Pi Interface
Stool & Analprint Analysis Module
Q1
Q2
Q3
G
D
NC
S
NFET
LED Control

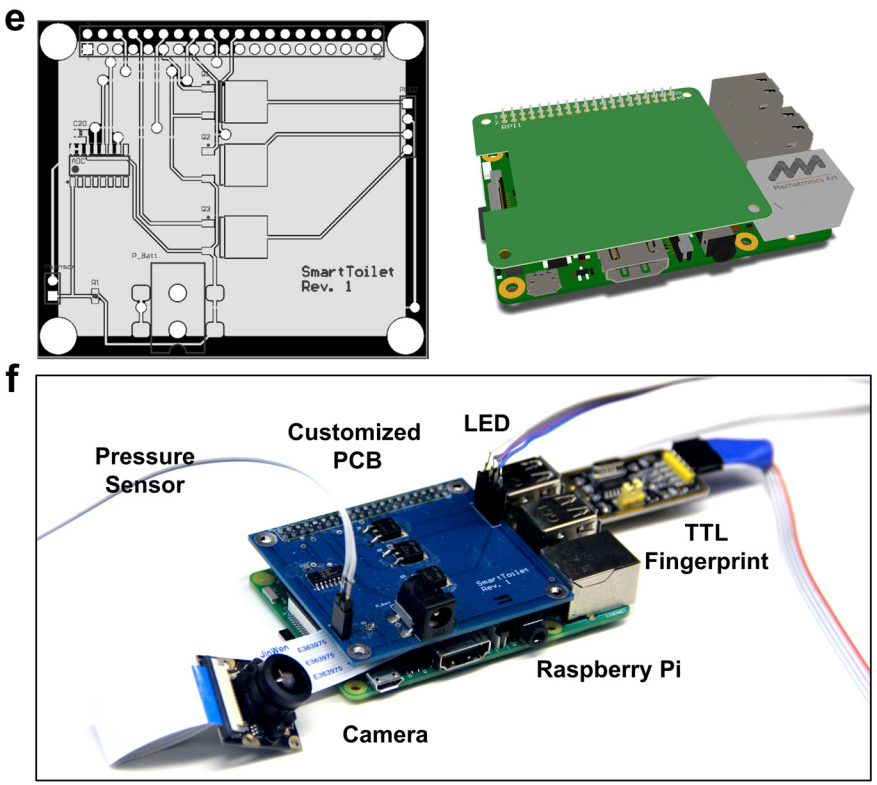

Supplementary Figure 9. a. Schematic wire-diagram for the urinalysis module. **b**. When the PIR motion sensor detects a urination event, a mounted strip is deployed by the uni-polar stepper motor (left). After a certain amount of time, the strip is retracted and recorded by the video camera (right). **c**. Schematic printed circuit board (PCB) layout (left) and its 3-D representation (right). **d**. Schematic wire-diagram for the stool & analprint analysis module. **e**. Schematic PCB (layout) and its 3-D representation how the PCB is integrated with a microprocessor. **f**. A picture of the PCB on top of the Raspberry Pi with the stool camera, pressure sensor, fingerprint transistor-transistor logic (TTL) serial, and light emitting diodes (LED).

References

1. Lewis, S.J. & Heaton, K.W. Stool form scale as a useful guide to intestinal transit time. *Scand J Gastroenterol* **32**, 920-924 (1997).
2. Mearin, F.*, et al.* Clinical Practice Guideline: Irritable bowel syndrome with constipation and functional constipation in the adult. *Rev Esp Enferm Dig* **108**, 332-363 (2016).
3. Sperber, A.D.*, et al.* The global prevalence of IBS in adults remains elusive due to the heterogeneity of studies: a Rome Foundation working team literature review. *Gut* **66**, 1075-1082 (2017).
4. Lacy, B.E. & Patel, N.K. Rome Criteria and a Diagnostic Approach to Irritable Bowel Syndrome. *J Clin Med* **6**(2017).
5. Palsson, O.S., Baggish, J. & Whitehead, W.E. Episodic nature of symptoms in irritable bowel syndrome. *Am J Gastroenterol* **109**, 1450-1460 (2014).
6. Palsson, O.S., Baggish, J.S., Turner, M.J. & Whitehead, W.E. IBS patients show frequent fluctuations between loose/watery and hard/lumpy stools: implications for treatment. *Am J Gastroenterol* **107**, 286-295 (2012).
7. Halmos, E.P.*, et al.* Inaccuracy of patient-reported descriptions of and satisfaction with bowel actions in irritable bowel syndrome. *Neurogastroenterol Motil* **30**(2018).
8. Self, M.M., Williams, A.E., Czyzewski, D.I., Weidler, E.M. & Shulman, R.J. Agreement between prospective diary data and retrospective questionnaire report of abdominal pain and stooling symptoms in children with irritable bowel syndrome. *Neurogastroenterol Motil* **27**, 1110-1119 (2015).

9. Chumpitazi, B.P.*, et al.* Bristol Stool Form Scale reliability and agreement decreases when determining Rome III stool form designations. *Neurogastroenterol Motil* **28**, 443-448 (2016).
10. Blake, M.R., Raker, J.M. & Whelan, K. Validity and reliability of the Bristol Stool Form Scale in healthy adults and patients with diarrhoea-predominant irritable bowel syndrome. *Aliment Pharmacol Ther* **44**, 693-703 (2016).
11. Hoshino, N.*, et al.* Effect of Daikenchuto (TJ-100) on gastrointestinal symptoms following laparoscopic colectomy in patients with colon cancer: study protocol for a randomized controlled trial. *Trials* **18**, 553 (2017).
12. Akamaru, Y.*, et al.* Effects of daikenchuto, a Japanese herb, on intestinal motility after total gastrectomy: a prospective randomized trial. *J Gastrointest Surg* **19**, 467-472 (2015).
13. Roman, H.*, et al.* Long-term functional outcomes following colorectal resection versus shaving for rectal endometriosis. *Am J Obstet Gynecol* **215**, 762 e761-762 e769 (2016).
14. Bertelsen, C.A.*, et al.* Long-term Functional Outcome After Right-Sided Complete Mesocolic Excision Compared With Conventional Colon Cancer Surgery: A Population-Based Questionnaire Study. *Dis Colon Rectum* **61**, 1063-1072 (2018).
15. Andreyev, J.*, et al.* Guidance on the management of diarrhoea during cancer chemotherapy. *Lancet Oncol* **15**, e447-460 (2014).
16. Hanai, A.*, et al.* Effects of a self-management program on antiemetic-induced constipation during chemotherapy among breast cancer patients: a randomized controlled clinical trial. *Breast Cancer Res Treat* **155**, 99-107 (2016).

17. Bonet, M.*, et al.* Assessment of acute bowel function after radiotherapy for prostate cancer: Is it accurate enough? *Clin Transl Oncol* **20**, 576-583 (2018).
18. Bruin, F.*, et al.* Laxative co-medication and changes in defecation patterns during opioid use. *J Oncol Pharm Pract*, 1078155218801066 (2018).
19. Farmer, A.D.*, et al.* Pathophysiology, diagnosis, and management of opioid-induced constipation. *Lancet Gastroenterol Hepatol* **3**, 203-212 (2018).
20. LoCasale, R.J., Datto, C., Wilson, H., Yeomans, K. & Coyne, K.S. The Burden of Opioid-Induced Constipation: Discordance Between Patient and Health Care Provider Reports. *J Manag Care Spec Pharm* **22**, 236-245 (2016).
21. Coyne, K.S.*, et al.* Translating Clinical Findings into the Patient's Perspective: Post-hoc Pooled Analysis of Bowel Movement Changes as a Predictor of Improvement in Patients' Opioid-induced Constipation Symptoms and Outcomes. *Clin Ther* **39**, 75-88 (2017).
22. Drossman, D.A. Functional gastrointestinal disorders: history, pathophysiology, clinical features, and Rome IV. *Gastroenterology* **150**, 1262-1279. e1262 (2016).
23. Remes-Troche, J.M., Ozturk, R., Philips, C., Stessman, M. & Rao, S.S. Cholestyramine--a useful adjunct for the treatment of patients with fecal incontinence. *Int J Colorectal Dis* **23**, 189-194 (2008).
24. Landis, J.R. & Koch, G.G. The measurement of observer agreement for categorical data. *biometrics*, 159-174 (1977).
25. Matthews, B.W. Comparison of the predicted and observed secondary structure of T4 phage lysozyme. *Biochimica et Biophysica Acta (BBA)-Protein Structure* **405**, 442-451 (1975).

26. Gorodkin, J. Comparing two K-category assignments by a K-category correlation coefficient. *Comput Biol Chem* **28**, 367-374 (2004).
27. Jurman, G., Riccadonna, S. & Furlanello, C. A comparison of MCC and CEN error measures in multi-class prediction. *PLoS One* **7**, e41882 (2012).
28. Wei, J.-M., Yuan, X.-J., Hu, Q.-H. & Wang, S.-Q. A novel measure for evaluating classifiers. *Expert Systems with Applications* **37**, 3799-3809 (2010).
29. Szegedy, C., Vanhoucke, V., Ioffe, S., Shlens, J. & Wojna, Z. Rethinking the inception architecture for computer vision. in *Proceedings of the IEEE conference on computer vision and pattern recognition* 2818-2826 (2016).
30. Ronald, J.A., Chuang, H.-Y., Dragulescu-Andrasi, A., Hori, S.S. & Gambhir, S.S. Detecting cancers through tumor-activatable minicircles that lead to a detectable blood biomarker. *Proceedings of the National Academy of Sciences* **112**, 3068-3073 (2015).
31. Aalipour, A.*, et al.* Engineered immune cells as highly sensitive cancer diagnostics. *Nat Biotechnol* **37**, 531-539 (2019).
32. Kwong, G.A.*, et al.* Mass-encoded synthetic biomarkers for multiplexed urinary monitoring of disease. *Nat Biotechnol* **31**, 63-70 (2013).